Roughness Effects on the Tip Vortex Strength and Cavitation Inception

Sixth International Symposium on Marine Propulsors
smp'19, Rome, Italy, May 2019

Roughness Effects on the Tip Vortex Strength and Cavitation Inception

Abolfazl Asnaghi[1], Urban Svennberg[2], Robert Gustafsson[2], Rickard E. Bensow[1]

[1]Department of Mechanics and Maritime Sciences, Chalmers University of Technology, Sweden
[2]Kongsberg Hydrodynamic Research Centre, Kongsberg Maritime Sweden AB, Kristinehamn, Sweden

ABSTRACT

The possibility and effectiveness of roughness application to mitigate tip vortex flows are evaluated by numerical simulations of an elliptical foil. The analysis includes investigation of the roughness size and area covered by the roughness, as well as the impact on the cavitation inception. Implicit Large Eddy Simulation (ILES) in OpenFOAM has been employed along with a wall-function incorporating the roughness effects to conduct the simulation on a proper grid resolution having the tip vortex spatial resolution as fine as 0.062 mm. The impact of the roughness size on the tip vortex is noted, and it is observed that for the studied condition, the roughness size of 250 μm is sufficient. The negative effects of roughness on the forces are also observed where application of roughness leads to lower lift and higher drag forces. To minimize the negative effects of the roughness on the performance, the roughness area optimization is conducted and it is found that the application of roughness on the leading edge and trailing edge of the suction side are acceptable to mitigate the tip vortex and also to limit the performance degradation. This is regarded to be in close relation with the way that the tip vortex forms in the studied operating condition. The study shows while the inception occurs at $\sigma = 6.35$ in the smooth condition, application of the roughness on the optimum area will delay the inception to $\sigma = 4.1$ while only increasing the drag coefficient 1.7%. This is found to be in a good agreement with the experimental measurements.

Keywords

Tip vortex, cavitation, mitigation, inception, roughness.

1 INTRODUCTION

In cavitation research and propeller design, tip vortex characteristics have a direct impact on the tip vortex cavitation (TVC) inception which itself is important in defining the boundaries of the cavitation free bucket chart of a propeller. In general, an efficient propeller has a highly loaded tip. This leads to more pronounced tip vortex structures which subsequently causes stronger tip vortex cavitation, hull excitation and rudder erosion. As TVC is usually the first type of cavitation that appears on a propeller, it plays a key role in initiating an overall increasing sound pressure level, and determining the underwater radiated noise (Wijngaarden et al. 2005, Bosschers 2018). The radiated noise is of big importance because it can disturb animals like whales and reduces comfort of people on board ship.

Several approaches are proposed and tested to modify tip vortex structures in order to prevent or at least delay tip vortex cavitation inception. Among these approaches, the application of roughness is a promising way (Kruger et al. 2016). Surface roughness affects the tip vortex roll-up as the roughness elements promote transition to turbulence in laminar boundary layers and therefore, alter the near-wall flow structures. The vortical structures generated by the roughness elements interact with the main tip vortex and destabilize it. If size, pattern, and location of roughness elements are selected appropriately, the destabilization process leads to tip vortex breakdown, and consequently leads to TVC mitigation.

In our previous studies, numerical simulations of tip vortex flows around a smooth elliptical foil were carried out, and successfully compared with experimental measurements (Asnaghi et al. 2017 and Asnaghi et al. 2018b). This type of foil has similar tip vortex behaviour as a propeller making it a suitable benchmark for both numerical and experimental investigations of cavitating tip vortex flows (Pennings et al. 2015). The aim of the present study is to provide further knowledge about the effects of the surface roughness on the TVC and the possibility of using roughness to delay the cavitation inception. The main focus is to find the most effective roughness size, and optimize the area where the roughness is applied in order to have a reasonable balance between the tip vortex mitigation and performance degradation.

To solve the flow field and turbulence, wall modelled ILES is employed. In this approach, the turbulent viscosity wall function is modified based on the non-dimensionalized roughness height to include the roughness effects (Tapia 2009). The simulations are conducted on a spatial grid having the wall-normal resolution $y^+ = 35$. This grid resolution satisfies the minimum requirements of tip vortex simulations using OpenFOAM according to our previous studies guidelines (Asnaghi 2018 and Asnaghi et al. 2018a), where at least 32 grid points across the vortex diameter is provided.

The investigation contains the impact of roughness on formation of vortical structures, their interactions and effects on the main tip vortex, as well as on TVC mitigation. Different roughness sizes ranging from 10 μm to 500μm are considered, and their impact on the cavitation inception

*

is evaluated. The difference in the flow pattern such as the leading edge vortex roll-up, angular momentum transportation, pressure and viscosity distributions between the rough and smooth foil surface conditions are analyzed. To minimize the negative effects of the roughness on the performance, the roughness area is optimized by simultaneous consideration of the tip vortex mitigation, performance degradation and their compromise. The results indicate that for the tested condition as the tip vortex forms on the suction side of the foil, the optimum area to apply the roughness is the leading edge and trailing edge of the suction side.

2 EQUATIONS

The flow over rough surfaces based on equivalent sand grain height, i.e. non-dimensional roughness height, can be classified into three regimes. In the smooth regime, the roughness elements are embedded in the viscous sublayer and consequently the friction drag is not affected by the roughness. In the fully rough regime, the viscous sublayer disappears and the friction drag significantly increases. The wall skin friction and the roughness impact become independent of Reynolds number which means the viscous effect is no longer important. The drag increase is only due to pressure forces on the roughness elements. The transition regime is between these two regimes where both viscous and pressure forces on the roughness elements contribute to the wall skin friction and drag.

The nondimensional roughness height to characterize the flow regime can be presented by $K_s^+ = u_\tau K_s/\nu$ where K_s is the roughness height, $u_\tau = \sqrt{\tau_w/\rho}$ is the shear velocity, and τ_w is the wall shear stress. In this study, we employ $K_s^+ = 2.5$ and $K_s^+ = 90$ as the limits of the transitional regime. Therefore, the flow regime is presented by,

$$\begin{cases} K_s^+ \leq 2.5 & \text{smooth} \\ 2.5 < K_s^+ < 90 & \text{transitionally rough} \\ 90 \leq K_s^+ & \text{fully rough} \end{cases}. \quad (1)$$

To model the roughness effect, the wall function developed by Tapia (2009) for the inner region of the turbulent boundary layer or the log-law region (e.g. $11 \leq y^+$ in OpenFOAM wall functions) is used,

$$u^+ = \frac{1}{\kappa}\ln(Ey^+) - \Delta B, \quad (2)$$

with the von Karman constant $\kappa = 0.41$, the constant E=9.8, the dimensionless wall distance $y^+ = u_\tau y/\nu$, and the velocity shift correction ΔB due to the roughness elements. In this approach, the height of the elements should be smaller than the height of the cells adjacent to the wall, i.e. $K_s^+ \leq y^+$. Otherwise, the part of roughness elements located outside the adjacent cells will not be included in the modelling.

In a smooth regime represented by $K_s^+ \leq 2.5$, the correction ΔB is set to zero and the wall function recalls the smooth wall function. For a transitionally rough regime where $2.5 < K_s^+ < 90$, the correction reads,

$$\Delta B = \frac{1}{\kappa}\ln\left[\frac{K_s^+ - 2.25}{87.75} + C_s K_s^+\right].\sin\big(A\big), \quad (3)$$

where $A = 0.425[\ln(K_s^+) - 0.811]$, and C_s is a constant representing shape and form of roughness elements. However, there is no guideline to adjust this coefficient. It is suggested that it varies from 0.5 to 1 where $C_s = 0.5$ corresponds to the uniformly distributed sand grain roughness. If the roughness elements deviate from the sand grains, the constant roughness should be adjusted by comparing the results with experimental data.

For a fully rough regime having $90 \leq K_s^+$, the ΔB correction is represented by,

$$\Delta B = \frac{1}{\kappa}\ln\left[1 + C_s K_s^+\right]. \quad (4)$$

The turbulent viscosity of cells adjacent to the rough wall is then recalculated using the following formula,

$$\mu_t = \mu\left[\frac{y^+\kappa}{\ln(Ey^+/e^{\kappa\Delta B})} - 1\right]. \quad (5)$$

To model the flow field by using LES approach, the low pass filtered equations of mass and momentum are employed,

$$\frac{\partial \rho_{\mathrm{m}}}{\partial t} + \frac{\partial(\rho_{\mathrm{m}}\bar{u}_i)}{\partial x_i} = 0, \quad (6)$$

$$\frac{\partial(\rho_{\mathrm{m}}\bar{u}_i)}{\partial t} + \frac{\partial(\rho_{\mathrm{m}}\bar{u}_i\bar{u}_j)}{\partial x_j} = -\frac{\partial \bar{p}}{\partial x_i} + \frac{\partial}{\partial x_j}(2\mu\bar{S}_{ij} - B_{ij}) + \rho_{\mathrm{m}} g_i, \quad (7)$$

where the over bar denotes low pass filtered quantities, and $B_{ij} = \rho(\overline{u_i u_j} - \bar{u}_i\bar{u}_j)$ is the subgrid stress tensor. The strain rate tensor, S_{ij}, is the symmetric part of the velocity gradient,

$$\bar{S}_{ij} = \frac{1}{2}\left(\frac{\partial \bar{u}_i}{\partial x_j} + \frac{\partial \bar{u}_j}{\partial x_i}\right). \quad (8)$$

In ILES, no explicit model is applied for B_{ij}, instead the numerical dissipation is considered enough to mimic the action of B_{ij} (Bensow & Fureby 2007, Fureby 2007, Bensow & Bark 2010).

The second invariant of velocity, Q-criterion, which represents the local balance between shear strain rate and rotational tensor magnitude, is employed to identify vortical structures in the flow,

$$Q = \frac{1}{2}(\bar{\Omega}_{ij}\bar{\Omega}_{ij} - \bar{S}_{ij}\bar{S}_{ij}), \quad (9)$$

where

$$\bar{\Omega}_{ij} = \frac{1}{2}\left(\frac{\partial \bar{u}_i}{\partial x_j} - \frac{\partial \bar{u}_j}{\partial x_i}\right). \quad (10)$$

3 CASE DESCRIPTION

The tip vortex flow around an elliptical foil is selected as a test case in order to gain insight about the impact of roughness on the flow pattern and tip vortex properties. The geometry of the foil is an elliptical planform having the

NACA $66_2 - 415$ cross section. The geometry and conditions are selected according to the experimental study conducted in the cavitation tunnel in the Laboratory for Ship Hydrodynamics at Delft Technical University (Pennings et al. 2015). The trailing edge of the tested foil is truncated at a thickness of 0.3 mm due to manufacturing limitations where the root chord length after truncation is $C_0 = 0.1256$ m. The total area of the foil obtained from the 3D CAD model is 0.01465 m^2 which is used as the reference area to compute non-dimensional parameters, e.g. lift coefficient. The foil has a half span of 150 mm, so that the tip is positioned in the centre of the test section. The foil is also placed in the middle of the channel width where distance to each side is equal to 150 mm. The simulations are conducted at the angle of attack equal to 9 degrees and a constant inlet velocity of 6.8 m/s. The outlet boundary is set as a fixed pressure boundary, and no-slip conditions are applied on the foil and bottom surfaces. The other boundaries are treated as slip conditions.

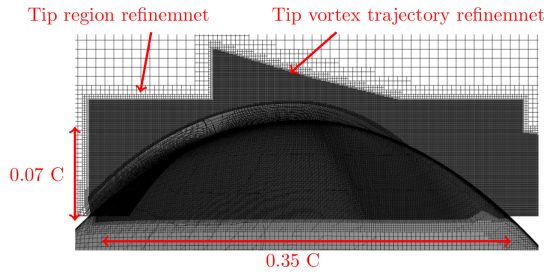

(a) Resolution around the tip, zoomed view

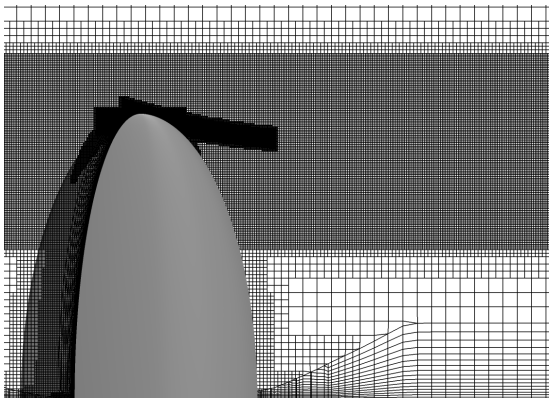

(b) Streamwise mesh distribution

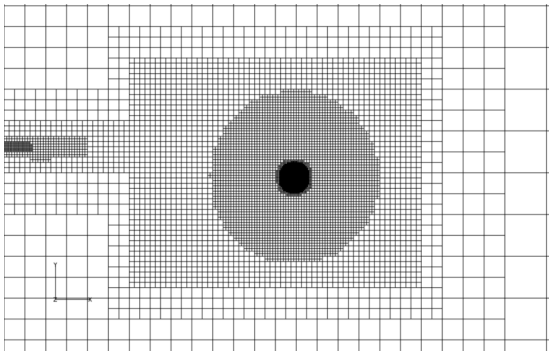

(c) Inplane mesh distribution

Figure 1: Mesh distribution in the streamwise and inplane directions.

The numerical results are compared with the recent experimental measurements conducted at the Rolls-Royce Hydrodynamic Research Center (RRHRC), Kristinehamn, Sweden. The foil used in the RRHRC experimental tests has a scale ratio of 2.4 compared to the one tested at TU Delft. However, the Reynolds number is kept the same to minimize the scale effect, and provide the opportunity to compare the results.

In Figure 1, distribution of computational cells in the streamwise and cross sections is presented. Several grid refinements are employed to provide a specific resolution in the tip vortex trajectory. In the streamwise and cross section directions, the maximum cell sizes are 0.125 mm and 0.0625 mm which follows our previous findings to have at least 32 grid points across the vortex diameter to predict a tip vortex flow using implicit LES in the OpenFOAM framework (Asnaghi 2018). The baseline mesh resolution on the foil surface has both x^+ and $z^+ < 250$, but considerably finer in the refined tip region. The spatial resolution at the foil tip region follows the tip vortex refinement, Figure 1a, providing a more suitable resolution for a wall modeled LES in this region. The prismatic cells consist of 20 layers having the wall normal resolution around $y^+ = 35$.

The OpenFOAM package, used in this study for numerical simulations, is an open source code written in C++ to model and simulate fluid dynamics and continuum mechanics. In OpenFOAM, the spatial discretization is performed using a cell−centred collocated finite volume (FV) method for unstructured meshes with arbitrary cell shapes, and a multi-step scheme is used for the time derivatives.

The PIMPLE algorithm is used to solve the coupling between the velocity and pressure. The solver tolerances, based on the residuals of pressure and velocity equations in each iteration, is set equal to 10^{-7}. The divergence terms are computed by employing a vector based TVD limited second order scheme. The gradients have been corrected to consider the non-orthogonality of the computational cells.

4 RESULTS

4.1 Smooth Foil

Formation of a tip vortex depends on the boundary layer development on both suction side and pressure side. Interactions of these two boundary layers and the trailing vortices determine the tip vortex strength and therefore its pressure distribution. In order to optimize the roughness area, it is essential to know which areas of the foil convey more momentum into the tip vortex. Distribution of vortical structures and flow streamlines are indications that can be considered to find the effective areas in the tip vortex formation and development.

The distribution of vortical structures, Figure 2, includes the pressure side and suction side views along with their tip zoomed views. The thick and thin lines plotted on the foil represent the distance of 0.1 C and 0.025 C, respectively.

The vortical structures on the suction side of the foil are formed mostly on the leading edge and the trailing edge.

The trailing vortices seem to be more interactive with the region that the minimum tip vortex pressure happens, $0.1 < z/C < 0.15$. The pressure side view shows that the vortical structures are generated on a small region at the very top of the foil.

The flow streamlines that pass through the tip vortex region at the section $z/C = 0.5$ are presented in Figure 3. The streamlines are plotted separately for the flow that goes inside the vortex core, blue lines, and for the flow that forms the outer region around the vortex core, red lines. The figure shows that the suction side leading edge streamlines mostly form the tip vortex core rather than the outer region. The pressure side streamlines seem to feed both the vortex core and the outer region.

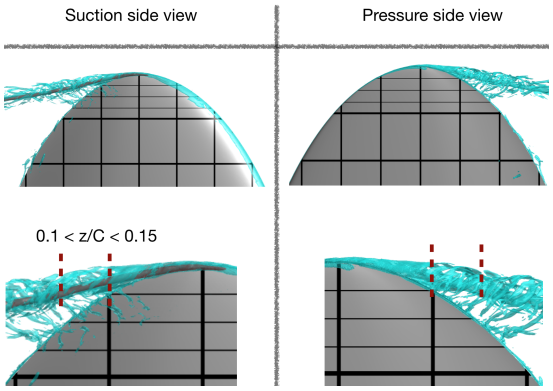

Figure 2: Distribution of the iso-surface Q=800 on the suction side and pressure side of the smooth foil.

It can be concluded that the effective areas on the tip vortex formation are the leading edge of both sides, and the trailing region of the suction side. We will use the following notations for these areas in the roughness area optimization: suction side leading edge, SSLE; suction side trailing edge, SSTE; and pressure side leading edge, PSLE.

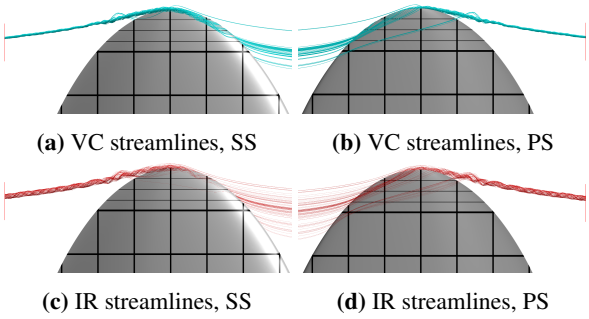

(a) VC streamlines, SS **(b)** VC streamlines, PS

(c) IR streamlines, SS **(d)** IR streamlines, PS

Figure 3: Flow streamlines passing through the vortex core (VC) and outer region (IR) around it at the section $z/C = 0.5$ of the smooth foil. SS: suction side, PS: pressure side.

4.2 Roughness Evaluation

We start the analysis of the roughness effects by examining a fully rough foil. Different roughness heights are considered ranging from 10 μm to 500 μm. Cavitation inception based on the minimum pressure is regarded as a criterion to compare different roughness heights in terms of tip vortex mitigation, Figure 4. As the results demonstrate, application of roughness leads to a weaker tip vortex compared to the smooth foil. The cavitation inception, which represents the strength of the tip vortex, decreases as the roughness height increases. For the considered condition, small changes are observed for roughness heights larger than 250 μm. Consequently, this roughness height is selected for the roughness area optimization.

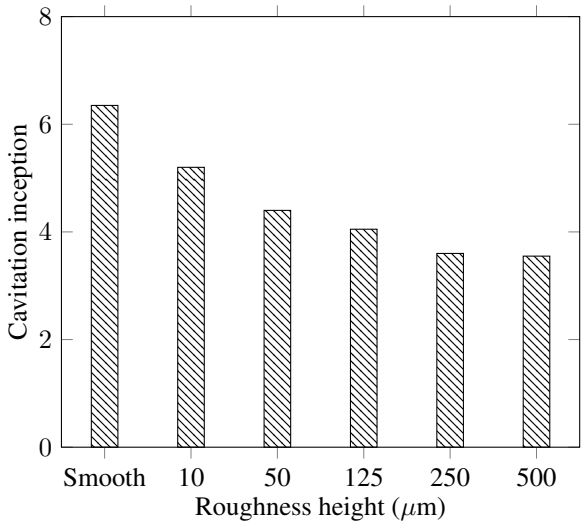

Figure 4: Variation of the cavitation inception versus the surface roughness height for the fully rough foil.

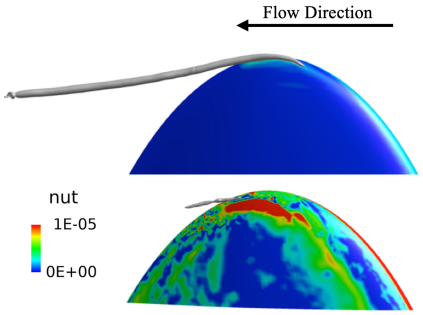

Figure 5: Comparison of the pressure coefficient iso-surface (C_p=-2.4) as an indication of the tip vortex strength between the smooth surface (upper figure) and rough surface (lower figure). The foil surface is colored with the turbulent viscosity. Roughness height is 250 μm. Suction side view.

The iso-surface of pressure coefficient is used in Figure 5 to represent the tip vortex strength in the smooth and fully rough (FR) foil conditions. Distribution of the turbulent viscosity on the foil indicates a region with very high turbulent viscosity close to the tip in the FR condition. The distribution of the pressure over the foil surface, Figure 6, shows that as roughness increases the turbulent viscosity over the surface, it alters the boundary layer distribution and consequently the pressure distribution. While in the

smooth condition, a strong low pressure region at the tip of the foil is clear, in the FR condition the pressure is more evenly distributed.

As pressure and turbulent viscosity change in the FR condition compared to the smooth condition, the flow streamlines that form the tip vortex also change, Figure 7. In the smooth surface condition, the streamlines are concentrated at the tip and form a leading edge vortex which initiates the tip vortex approximately at the section z/C=-0.05. In the FR case, the flow streamlines are distributed more evenly on the tip, and therefore, are not concentrated or strong enough to form the tip vortex right on the tip of the foil.

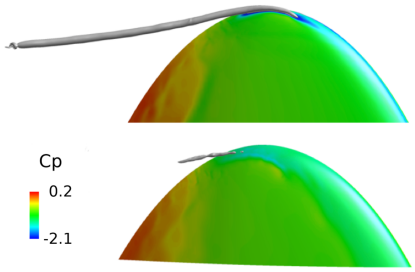

Figure 6: Comparison of the pressure distribution between the smooth surface (upper figure) and rough surface (lower figure). Roughness height is 250 μm. Suction side view.

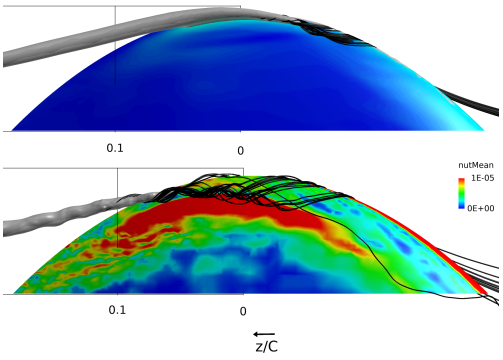

Figure 7: Comparison of the vortex core streamlines (black lines) between the smooth surface (upper figure) and rough surface (lower figure). Foil is colored by the turbulent viscosity. The tip vortex is represented by the iso surface of pressure C_p=-2.4. Roughness height is 250 μm. Suction side view.

In Figure 8, the isometric zoomed view of the suction side is presented. The inplane vector distribution at the section z/C=0 is included to provide further information of the angular momentum distribution between the smooth and FR conditions. As can be observed, in the smooth surface condition, the angular momentum is concentrated around a main vortex which initiates the tip vortex. A smaller vortex further down of the tip at this section is noticeable. However, as the small vortex and the main vortex are far from each other, and the small vortex is relatively weaker than the main vortex, it does not affect the tip vortex formation.

In the FR condition, the angular momentum is more evenly distributed. The results show the formation of two vortexes close to the tip where the tip vortex eventually initiates from the stronger vortex. Moreover, contradictory to the smooth foil condition, not all of the streamlines pass through the stronger vortex.

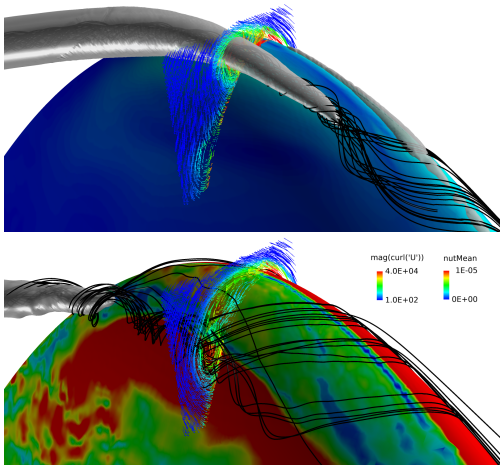

Figure 8: Comparison of the inplane velocity vectors at the section z/C=0 between the smooth surface (upper figure) and rough surface (lower figure). The other settings follow Figure 7. Isometric zoomed view of the tip suction side.

Surface roughness promotes the laminar boundary transition into turbulent flow which then leads to more frictional losses. The transition of the boundary layer also changes the pressure distribution over the foil. As a result of these two changes, rough foils usually have higher drag force and lower lift force compared to the smooth foil at the same condition. The roughness area optimization is conducted in a way to minimize the negative effects of the roughness on the performance while keeping the tip vortex strength as low as possible. In this study, the roughness area optimization is limited to the regions that are highlighted in the smooth foil analysis, i.e. SSLE, PSLE, and SSTE. Different cases containing different combinations of these roughness areas are constructed, Table 1.

Table 1: Case description of different roughness areas.

Case	(I)	(II)	(III)	(IV)	(V)
Roughness areas	SSLE	PSLE	SSLE PSLE	SSLE SSTE	SSLE SSTE PSLE

In Table 2, the lift and drag forces of these cases are presented. The values are normalized by the smooth foil forces, and are presented as the percentage of increase for drag force and percentage of decrease for the lift force. The results of the FR foil is also included in this table as the reference of the extreme performance degradation condition.

Table 2: Percentage of the drag and lift forces variations relative to the smooth foil condition. Roughness height = 250 μm.

Case	Increased drag force(%)	Decreased lift force(%)
(I)	0.8	0.04
(II)	10.5	0.93
(III)	16.9	1.51
(IV)	1.7	0.07
(V)	9.0	0.81
FR	85.7	6.51

As discussed before, it is observed that having roughness all over the foil increases the drag force by 85.7% and decreases the lift force by 6.51%. The predicted force variations of the limited roughness area cases show a lower negative impact of the roughness on the performance. Also, it can be noted that having roughness on the pressure side, i.e. case (II),(III), and (V), contributes more to the performance degradation. Among the cases, the highest increased drag force is for case (III) where the roughness is applied on the leading edges of the suction side and pressure side. Inclusion of roughness on the SSTE, i.e. case (V), somehow reduces the negative impact of the roughness on the forces. The results clarify that having roughness only on the suction side, case (I) and (IV), are favourable in terms of the forces evaluation of the roughness impact.

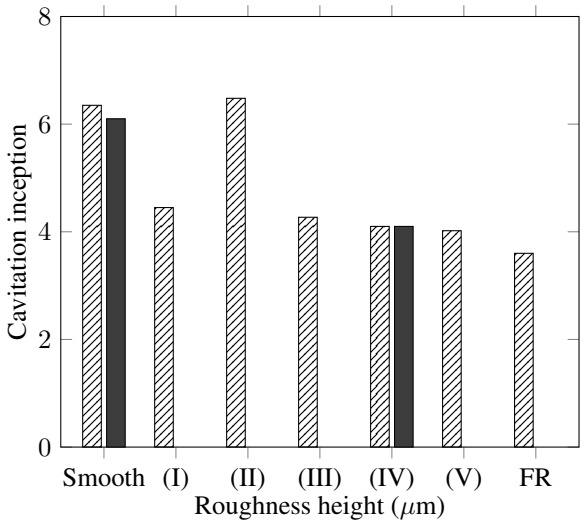

Figure 9: Variation of the cavitation inception versus different surface roughness areas, FR: fully rough foil, roughness height = 250 μm, solid bars (smooth and (IV)) are the experimental measuremnets.

The predicted cavitation inception of the cases is presented in Figure 9, and is compared with the experimental measurements. In case (II) where the roughness is applied only on the pressure side, the tip vortex strength is not reduced. This suggests the necessity of having roughness on the side where the tip vortex forms, e.g. suction side in our study. Among the studied cases, the lowest cavitation inception points belong to the case (V), and then case (IV). However, as the performance degradation is much lower in case (IV), this case is considered as the outcome of the roughness area optimization. The comparison between the numerical results (bars with dashed lines) and the experimental measurements (bars with the solid color) shows a very good agreement. It clearly highlights the capability of the current method in modelling the roughness and its impact on the tip vortex cavitation.

CONCLUSIONS

The results on the evaluated elliptical foil show that the application of roughness in order to mitigate a tip vortex is very promising. It is found that the roughness size and the area that the roughness are applied have a direct impact on the interactions between the roughness elements and boundary layers over the foil, and eventually on the strength of the tip vortex.

The results indicate that increasing the size of roughness until a certain size, i.e. 250 μm, leads to a weaker tip vortex in the studied condition and after that using bigger roughness sizes does not affect the flow field.

Since roughness elements increase turbulent viscosity over the surface, they alter the boundary layer distribution and consequently the pressure distribution on the foil. This affects formation of the leading edge vortex and therefore, the position and strength of the tip vortex. While in the smooth surface condition, a low pressure region at the tip of the foil is visible, in the fully rough foil condition the pressure at the tip of the suction side is more evenly distributed. This is noted to be responsible for a more even distribution of the angular momentum over the tip of the foil in the rough foil condition.

The negative effects of roughness on the performance, i.e. having lower lift and higher drag forces, are observed in the rough foil conditions. As an instance, for the fully rough foil with the roughness height of 250 μm, the lift and drag forces are decreased by 6.51% and increased by 85.7% compared to the smooth foil condition. This emphasize the necessity of optimizing the areas covered by the roughness.

The streamlines and vortical structures distributions show that the flow over the leading edges of the suction side and pressure side, and also the trailing edge of the suctions side are more important in the tip vortex formation and its development. Consequently, optimization of roughness area are limited to these regions. By considering the cavitation inception and the predicted forces, it is concluded that for the tested condition the optimum area to apply the roughness is the leading edge and trailing edge of the suction side. However, it should be considered that this finding is stricly limited to the way that the tip vortex is formed in the studied condition, i.e. having a vortex roll-up on the suction side leading edge. The comparison between the numerical results and the experimental measuremnets recently conducted at the Rolls-royce Hydrodynamics Research Center clearly shows the capability of the numerical methodology to model the roughness impact on the tip vportex formation. It also highlightes the possibility of roughness appli-

cation in tip vortex mitigation.

ACKNOWLEDGEMENTS

Financial support for this work has been provided by Vinnova through the RoughProp project, Grant number 2018-04085. The simulations were performed on resources at Chalmers Centre for Computational Science and Engineering (C3SE) provided by the Swedish National Infrastructure for Computing (SNIC).

REFERENCES

Asnaghi, A., Bensow, R.E. & Svennberg, U. (2017). 'Implicit Large Eddy simulation of tip vortex on an elliptical foil', Proceedings of Fifth Symposium on Marine Propulsion (SMP 2017), Espoo, Finland.

Asnaghi, A. (2018). 'Computational modelling for cavitation and tip vortex flows', PhD thesis, Chalmers University of Technology.

Asnaghi, A., Svennberg, U. & Bensow, R.E. (2018a). 'Numerical and experimental analysis of cavitation inception behaviour for high-skewed low-noise propellers', Applied Ocean Research **79**(1).

Asnaghi, A., Svennberg, U. & Bensow, R.E. (2018b). 'Analysis of tip vortex inception prediction methods', Ocean Engineering **167**(1).

Bensow, R.E. & Fureby, C. (2007). 'On the justification and extension of mixed methods in LES', J. Turbulence **8**(1).

Bensow, R.E. & Bark, G. (2010). 'Implicit LES predictions of the cavitating flow on a propeller', Journal of Fluids Engineering **132**(4).

Bosschers, J. (2018). 'Propeller tip-vortex cavitation and its broadband noise', PhD thesis, University of Twente.

Fureby, C. (2007). 'ILES and LES of Complex Engineering Flows', J. Fluids Eng. **129**(12).

Kruger, C., Kornev, N. & Greitsch, L. (2016). 'Influence of propeller tip roughness on tip vortex strength and propeller performance', Ship Technology Research **63**(2).

Pennings, P.C., Westerweel, J. & van Terwisga, T.J.C. (2015). 'Flow field measurement around vortex cavitation'. Experiments in Fluids **56**(11).

Tapia, X.P. (2009). 'Modelling of wind flow over complex terrain using OpenFoam', Master thesis, University of Gavle.

Wijngaarden, E.V., Bosschers, J. & Kuiper, G. (2005). 'Aspects of the cavitating propeller tip vortex as a source of inboard noise and vibration', Proceedings of FEDSM2005, ASME Fluids Engineering Division Summer Meeting and Exhibition, Houston, TX, USA.